

PAPER

Realistic anatomically detailed open-source spinal cord stimulation (RADO-SCS) model

To cite this article: Niranjan Khadka *et al* 2020 *J. Neural Eng.* **17** 026033

View the [article online](#) for updates and enhancements.



The Department of Bioengineering at the University of Pittsburgh Swanson School of Engineering invites applications from accomplished individuals with a PhD or equivalent degree in bioengineering, biomedical engineering, or closely related disciplines for an open-rank, tenured/tenure-stream faculty position. We wish to recruit an individual with strong research accomplishments in Translational Bioengineering (i.e., leveraging basic science and engineering knowledge to develop innovative, translatable solutions impacting clinical practice and healthcare), with preference given to research focus on neuro-technologies, imaging, cardiovascular devices, and biomimetic and biorobotic design. It is expected that this individual will complement our current strengths in biomechanics, bioimaging, molecular, cellular, and systems engineering, medical product engineering, neural engineering, and tissue engineering and regenerative medicine. In addition, candidates must be committed to contributing to high quality education of a diverse student body at both the undergraduate and graduate levels.

[CLICK HERE FOR FURTHER DETAILS](#)

To ensure full consideration, applications must be received by June 30, 2019. However, applications will be reviewed as they are received. Early submission is highly encouraged.



PAPER

Realistic anatomically detailed open-source spinal cord stimulation (RADO-SCS) model

RECEIVED
5 December 2019REVISED
18 March 2020ACCEPTED FOR PUBLICATION
25 March 2020PUBLISHED
23 April 2020Niranjan Khadka¹ , Xijie Liu¹, Hans Zander^{2,3} , Jaiti Swami¹, Evan Rogers^{2,3}, Scott F Lempka^{2,3,4} and Marom Bikson¹¹ Department of Biomedical Engineering, The City College of New York, CUNY, New York, United States of America² Department of Biomedical Engineering, University of Michigan, Michigan, United States of America³ BioInterfaces Institute, University of Michigan, Michigan, United States of America⁴ Department of Anesthesiology, University of Michigan, Michigan, United States of AmericaE-mail: bikson@ccny.cuny.edu and lempka@umich.edu**Keywords:** Spinal cord stimulation (SCS), detailed anatomy, finite element method, current-flow model, axon model**Abstract**

Objective. Computational current flow models of spinal cord stimulation (SCS) are widely used in device development, clinical trial design, and patient programming. Proprietary models of varied sophistication have been developed. An open-source model with state-of-the-art precision would serve as a standard for SCS simulation. *Approach.* We developed a sophisticated SCS modeling platform, named Realistic Anatomically Detailed Open-Source Spinal Cord Stimulation (RADO-SCS) model. This platform consists of realistic and detailed spinal cord and ancillary tissues anatomy derived based on prior imaging and cadaveric studies. In our finite element model of the T9-T11 spine levels, we represented the following tissues: vertebrae, intervertebral disc, epidural space, epidural space vasculature, dura mater, dural sac, intraforaminal tissue, cerebrospinal fluid (CSF), whitematter, spinal cord vasculature, Lissauer's tract, gray matter, dorsal and ventral roots and rootlets, dorsal root ganglion (DRG), sympathetic chain (trunk and ganglion), thoracic aorta and its branching, peripheral vasculature, and soft tissues (thorax). As an exemplary application to illustrate the model workflow, we simulated a bipolar SCS montage and calculated the corresponding activation thresholds for individual axons populating the spinal cord. *Main results.* RADO-SCS provides state-of-the-art precision across 19 tissue compartments. The resulting model calculations of the electric fields generated in the white-matter and gray matter, and the axonal activation thresholds are broadly consistent with prior simulations. *Significance.* The RADO-SCS can be used to simulate any SCS approach with both unprecedented resolution (precision) and transparency (reproducibility). Freely-available online, the RADO-SCS will be updated continuously with version control.

1. Introduction**1.1. Broad impact of an open-source high-resolution computational SCS model**

Computational models predict current flow patterns and neuronal activation during neuromodulation techniques, such as spinal cord stimulation (SCS) [1–3]. These models are key tools in designing, optimizing, and understanding SCS as they relate the *controllable* stimulation dose (i.e. electrode placement and waveform [4]) with the *intended* resulting activation of the spinal cord and nerves [5, 6]. Computational SCS models thus broadly inform modern clinical SCS practices, ongoing research into

mechanisms of actions, and design of new interventions [2, 7–14].

Since the early 1980's, models of SCS have been continuously refined and applied [1, 2, 5, 11, 13–33] (see table 1). Development of models of increasing complexity offered mirrored general enhancements in numerical modeling techniques (finite element analysis), with proprietary efforts by numerous groups, each subject to multiple version iterations. Without open-source model-geometry and a standard modeling pipeline, exact replication is difficult. Indeed, the more advanced (detailed) a model, the more intractable the model is to reproduce without source code. Moreover, even recent models

can lack details of major anatomical structures of the spine.

Here, we develop the first open-source and the most precise structural model for SCS simulation, called the Realistic Anatomically Detailed Open-source Spinal Cord Stimulation (RADO-SCS) model. The RADO-SCS pipeline uses computer aided design (CAD) derived files of spinal tissues, along with available devices renders, meshes, finite element method (FEM) results, and axonal activation simulations. One exemplary SCS clinical lead was modeled and placed epidurally. However, users can redesign and position SCS leads based on any device and intervention specifics. Under a Creative Commons Attribution 4.0 International (CC BY 4.0) license, an open-source tissue anatomical mask and device model STL files of RADO-SCS 3.0 (current version) are available for free download from Zenodo.org (<https://doi.org/10.5281/zenodo.3715368>). Any model related inquiries or an additional model files download request are addressed through <https://www.neuralengr.org/spinal-cord-stimulation>. RADO-SCS supports simulation of any SCS dose (technology) and will be subjected to ongoing updates with version control in Zenodo.org.

RADO-SCS supports stimulation of any SCS dose (technology) and will be subject to ongoing updates with version control. The more precise and complex a computational model, the more critical it is to share code for reproducibility and to prevent a need to redo the resource-intensive creation effort. Use of RADO-SCS thus provides users with: (1) a transparent and reproducible platform to base any claims; (2) evolving state-of-the-art precision to the best model quality; and (3) cost and time savings. RADO-SCS is a unique tool for supporting computer-driven device design, dose optimization, and an efficient clinical trial design.

2. Methods

2.1. State-of-the-art RADO SCS model

Adding more details, increasing resolution and anatomical precision to earlier model versions [2, 7, 34], we developed the first RADO-SCS model, including additional spinal tissue compartments that were not previously developed/modelled. Adding these extra tissues will likely influence the current flow pattern from the SCS lead to the spinal cord or to another possible region of interest. We derived the dimensions and boundaries of tissue compartments of the RADO-SCS model from human cadaver studies, specifically from the lower thoracic spinal cord as discussed in our prior studies [2, 7, 35, 36]. In addition, we constructed some features, such as Lissauer's tract, thoracic aorta, sympathetic chains, dorsal and ventral roots, and rootlets based on physiological trajectory data [37]. The RADO-SCS model consists

of major spinal canal and peripheral tissue compartments with basic, moderate, and enhanced anatomical precision: vertebrae (moderate precision), intervertebral (IV) discs (moderate precision), epidural space (moderate precision), epidural space vasculature (basic precision), dura mater (moderate precision), dural sac (basic precision), intraforaminal tissue (basic precision), CSF (moderate precision), white-matter (enhanced precision), spinal cord vasculature (basic precision), Lissauer's tract (enhanced precision), gray matter (enhanced precision), dorsal and ventral root, rootlets (moderate precision), dorsal root ganglion (DRG) (moderate precision), sympathetic chain (trunk and ganglion) (basic precision), thoracic aorta and its branching (basic precision), peripheral vasculatures (basic precision), and soft tissues (basic precision) (figure 1).

Specifically, we modelled and positioned three vertebrae and IV discs to mimic the T9-T11 lower thoracic spine with an anatomical curvature and tissue specific flexion. We modelled four DRG lateral to the vertebrae (each side) in the rostral-caudal direction. The dorsal and ventral root converged together just beyond the DRG, while moving away from the cord to form a spinal nerve within the intervertebral foramen. These nerves and roots were surrounded by meninges and CSF. The dorsal and ventral rootlets emerged from the dorsal and ventral horn of the spinal cord. We constructed eight dorsal and eight ventral rootlets at each spinal level. We constructed the thoracic aorta (which supplies arterial blood to the spinal cord) and its anastomotic network of radicular arteries that run along the dorsal and ventral roots of the spinal nerves. The radicular arteries further branched at the spinal cord. We constructed two sympathetic chains (trunk and ganglion) and we connected the nerve from each sympathetic trunk to the spinal nerve. Next, we constructed the dural sac/covering, a membranous sheath that is part of the subarachnoid space, contains CSF, and surrounds the spinal cord. The outermost layer of the spinal tissue was an epidural space, which lies between dura mater and the vertebral wall and is a major spinal tissue compartment that predominantly contains fat. We modelled miniature blood vessels within the epidural space. Next, we constructed dura which is the outermost layer of the meninges. Inside the dura was a layer of conductive CSF, which mimics the subarachnoid space that exists between the arachnoid and the pia mater. The inner most constructed tissue compartments were white-matter and gray-matter domains representing the spinal cord. We also included Lissauer's tract, a white-matter pathway near the dorsal horn and lateral aspect of the dorsal columns. We then placed the T9-T11 thoracic spinal column inside a thorax/soft tissues. Finally, we modeled an eight-contact clinical SCS lead (diameter: 1.25 mm, electrode contact

Table 1. Comparison of the RADO SCS model with other existing SCS models based on model derivation (CAD vs. MRI), constructed tissue compartments (unclear, considered, and not considered/absent), and precision in anatomical details (limited, basic, moderate, and enhanced). Limited refers to SCS models with minimal anatomical precision in constructed tissue compartments. Basic precision SCS models have regular shapes (e.g. cylindrical, triangular, rectangular prisms, wedges, bricks, or cubes) as tissue compartments, no flexion in geometry, and uniform dimension across spine levels. Moderate precision SCS models include tissue compartments with minimal resolution or have regular geometric shapes with some flexion and uniform dimension across spine level. Enhanced precision refers to SCS models with tissue compartments with realistic geometry, additional anatomical details (flexion, bifurcation, union), high resolution, and spine level specific dimensions.

References	RADO-SCS	Anaya, 2019	Zannou, 2019	Graham, 2019
Model derivation	CAD derived	CAD derived	CAD derived	CAD derived
Spine level	T8-T11	Lower thoracic	T8-T11	L5
Tissue compartments				
Vertebrae	✓, MP	✓, MP	✓, MP	✓, BP
IV Disc	✓, MP	✓, MP	✓, MP	✗
Epidural space (predominantly fat)	✓, MP	✓, BP	✓, BP	✗
Dura mater/ Meninges/Dural sac	✓, MP	✓, BP	✓, BP	✓, BP
Cerebrospinal fluid (CSF)	✓, MP	✓, BP	✓, BP	✗
Spinal Cord	✓, EP	✓, EP	✓, BP	✗
White-matter	✓, EP	✓, EP	✗	✗
Gray-matter	✓, EP	✓, EP	✗	✗
Lissauer's tract	✓, EP	✗	✗	✗
Roots	✓, MP	✗	✓, BP	✓, BP
Ventral root	✓, MP	✗	✗	✗
Dorsal root	✓, MP	✗	✗	✓, BP
Dorsal root ganglion (DRG)	✓, MP	✗	✗	✓, BP
Dorsal and Ventral rootlets	✓, MP	✓, MP (Dorsal only)	✓, BP	✗
Intraforaminal tissue	✓, BP	✗	✗	✓, BP
Sympathetic chain (trunk, ganglion)	✓, BP	✗	✗	✗
Thoracic aorta and sub-vasculature	✓, BP	✗	✓, BP	✗
Epidural space vasculature	✓, BP	✗	✗	✗
White-matter vasculature	✓, BP	✗	✗	✗
Peripheral spinal tissues/thorax	✓, BP	✓, BP	✓, BP	✓, BP

Compartments: ✗, Not considered/Absent; ✓, Considered; , Unclear.

Anatomical details: LT, Limited; MP, Moderate precision; BP, Basic precision; EP, Enhanced precision.

Table 1. (Continued).

Anderson, 2019	Lempka, 2019	Durá, 2019	Fernandes, 2018, 2019	Wagner, 2018,	Kent, 2018	Arle, 2016, 2013
CAD derived	CAD derived	CAD derived	MRI derived	CAD derived	CAD derived	CAD derived
T8-T10	Lower thoracic	T10	Whole Spine	L1-S2	θ	θ; T8-T9 (2013)
✗	✓, MP	✓, BP	✓, EP	θ	✓, LT	✓, BP; ✗ (2013)
✗	✗	✗	✓, EP	θ	✗	✗
✓, BP	✓, BP	✓, BP	θ	✓, MP	✗	✓, BP
✓, BP	✓, BP	✓, BP	✓, EP	θ	✗	✓, BP
✓, BP	✓, MP	✓, BP	✓, EP	✓, MP	✗	✓, BP
✓, BP	✓, MP	✓, MP	✓, EP	✓, MP	✗	✓, BP
✓, BP	✓, MP	✓, MP	✓, EP	✓, MP	✗	✓, BP
✓, BP	✓, MP	✓, MP	✓, EP	✓, MP	✗	✓, BP
✗	✗	✗	✗	✗	✗	✗
✗	✓(Modeled as a cable)	✓, LT	✓, BP	✓, MP	✗	✓, BP; ✗ (2013)
✗	✗	✗	✓, BP	✓, MP	✗	✗
✗	✓ (DR fibers)	✓, (DR fibers)	✓, BP	✓, MP	✓, BP	✓, BP
✗	✗	✗	✗	✗	✓, BP	✗
✗	✗	✗	✗	✓, MP	✗	✗
✗	✗	✗	✗	✗	✓, LT	✗
✗	✗	✗	✗	✗	✗	✗
✗	✗	✗	✗	✗	✗	✗
✗	✗	✗	✗	✗	✗	✗
✗	✓, BP	✗	✓, EP	θ	✗	✓, BP

Table 1. (Continued).

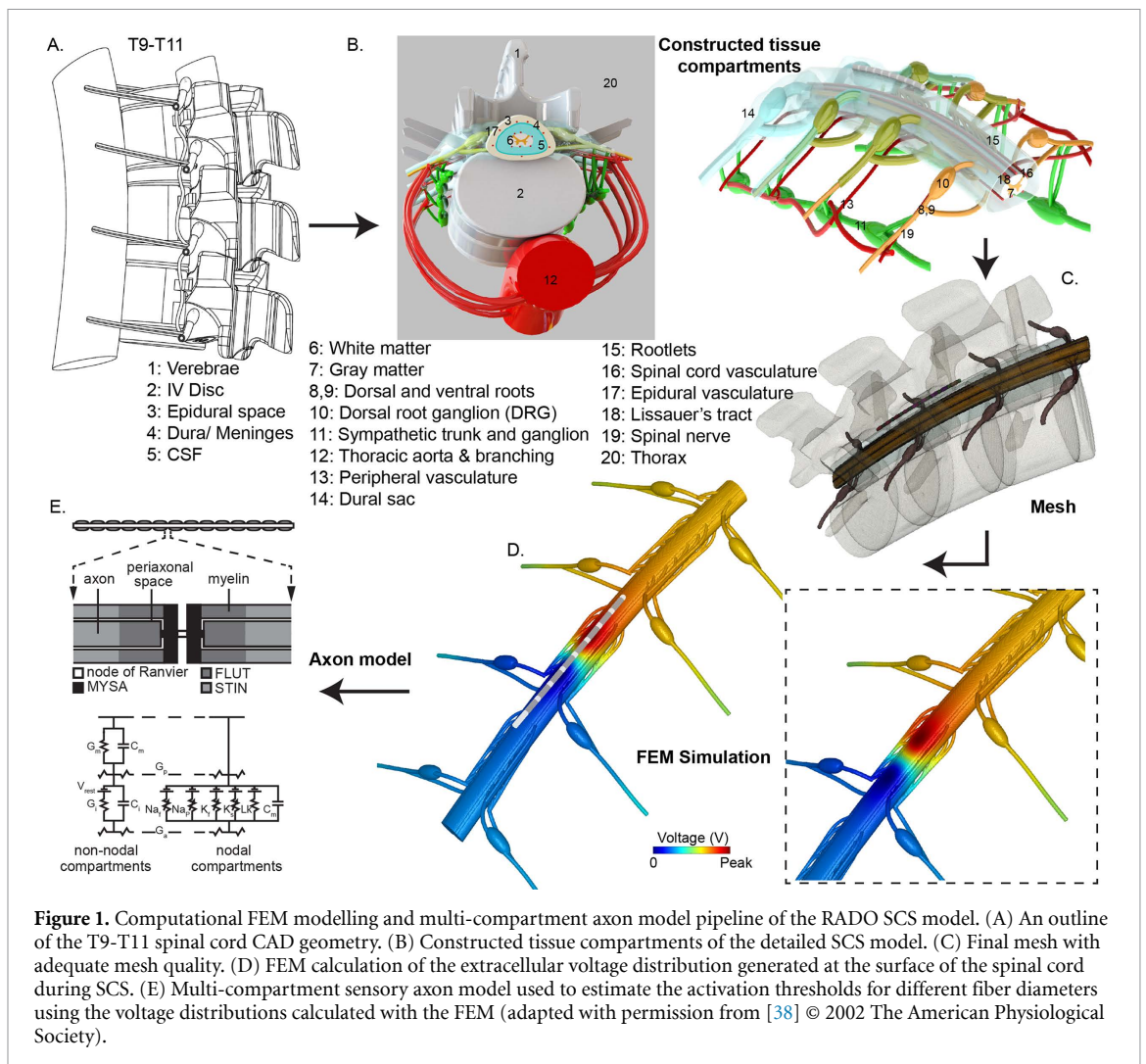
Lempka, 2015	Huang, 2014	Kent, 2014	Howell, 2014	Fiocchi S, 2016; Parazzini, 2014	Laird, 2013	H-Lábrádo, 2011
CAD derived	CAD derived	CAD derived	CAD derived	MRI derived	CAD derived	CAD derived
Lower thoracic	thoracic	T7-T10	T3-L2	Whole Spine	T10	C2-T1
✓, BP	✓, BP	✓, BP	✓, MP	✓, EP	✓, LT	✓, BP
✗	✗	✗	✓, MP	✓, EP	✗	✓, BP
✓, BP	✓, BP	✓, BP	✓, MP	∅	✓, LT	✓, BP
✓, BP	✓, BP	✗	✓, MP	✗	✗	✓, BP
✓, BP	✓, BP	✓, BP	✓, MP	✓, EP	✓, LT	✓, BP
✓, EP	✓, BP	✓, BP	✓, MP	✓, EP (Single compartment)	✓, LT	✓, BP
✓, EP	✓, BP	✓, BP	✓, MP	✗	✓, LT	✓, BP
✓, EP	✓, BP	✓, BP	✓, MP	✗	✓, LT	✓, BP
✗	✗	✗	✗	✗	✗	✗
✓, BP	✗	✗	✓ (Modeled as a cable)	✗	✓ (Modeled as a cable)	✗
✗	✗	✗	✗	✗	∅	✗
✓, BP	✗	✗	✓ (DR fibers)	✗	∅	✗
✗	✗	✗	✗	✗	✗	✗
✗	✗	✗	✗	✗	✗	✗
✗	✗	✗	✗	✗	✗	✗
✗	✗	✗	✗	✗	✗	✗
✗	✗	✗	✗	✗	✗	✗
✗	✗	✗	✗	✗	✗	✗
✓, BP	✗	✗	✓, BP	✓, EP	✗	✓, BP

Table 1. (Continued).

Veizi, 2017; Lee, 2011	Howard, 2011	Danner, 2011; Ladenbauer, 2010	Manola, 2007, 2004	Holsheimer, 2002	Rattay, 2000
CAD derived	CAD derived	CAD derived	CAD derived	CAD derived	CAD derived
T1- T12 & lower-lumbar and sacral	∅	T11- T12, L1-L4	∅	∅	T11-T12, L1-L2
✓, BP	✓, LT	✓, MP	✓, BP	✓, BP	✓, BP
✗	✗	✓, BP	✗	✗	✗
✓, BP	✓, LT	✓, BP	✓, BP	✓, BP	✓, BP
✓, BP	✗	✗	✓, BP	✗	✓, BP
✓, BP	✓, LT	✓, BP	✓, BP	✓, BP	✓, BP
✓, EP	✓, LT	✓, BP	✓, BP	✓, BP	✓, MP
✓, EP	✓, LT	✓, BP	✓, BP	✓, BP	✓, MP
✓, EP	✓, LT	✓, BP	✓, BP	✓, BP	✓, MP
✗	✗	✗	✗	✗	✗
✓ (Modeled as a cable)	✗	✓ (Modeled as a cable)	✓ (Modeled as a cable)	✓ (Modeled as a cable)	✓ (Modeled as a cable)
✗	✗	✓ (VR fiber)	✗	✗	✗
✓ (DR fibers)	✗	✓ (DR fiber)	✓ (DR fibers)	✓ (DR fibers)	✓ (DR fibers)
✗	✗	✗	✗	✗	✗
✗	✗	✗	✗	✗	✗
✗	✗	✗	✗	✗	✗
✗	✗	✗	✗	✗	✗
✗	✗	✗	✗	✗	✗
✗	✗	✗	✗	✗	✗
✓, BP	✗	✓, BP	✓, BP	✓, BP	✓, BP

Table 1. (Continued).

Wesselink, 1998, 1999; Holsheimer, 1995; Struijk, 1993a, 1993b	Struijk, 1991, 1992	Coburn and Sin, 1985	Sin and Coburn, 1983	Coburn, 1980
CAD derived	CAD derived	CAD derived	CAD derived	CAD derived
C4-C6, T4-T7, T10-T11	C5, C6	θ	θ	Thoracic
✓, BP	✗	✓, BP	✓, LT	✓, LT
✗	✗	✗	✗	✗
✓, BP	✓, BP	✓, BP	✓, LT	✓, LT
✓, BP	✗	✗	✗	✗
✓, BP	✓, BP	✓, BP	✓, LT	✓, LT
✓, BP	✓, BP	✓, BP	✓, LT	✓, LT
✓, BP	✓, BP	✓, BP	✓, LT	✓, LT
✓, BP	✓, BP	✓, BP	✓, LT	✓, LT
✗	✗	✗	✗	✗
✓ (Modeled as a cable)	✗	✓, BP	✗	✓, LT
✗	✗	✓, BP	✗	✓, LT
✓ (DR fibers)	✗	✓, BP	✗	✓, LT
✗	✗	✗	✗	✗
✗	✗	✗	✗	✗
✗	✗	✗	✗	✗
✗	✗	✗	✗	✗
✗	✗	✗	✗	✗
✗	✗	✗	✗	✗
✗	✗	✗	✗	✗
✗	✗	✗	✗	✗
✗	✗	✗	✗	✗
✓, BP	✓, BP	✓, BP	✓, LT	✓, LT



length: 3 mm, inter-electrode insulation gap: 1 mm) (figure 2) and placed it 1 mm distal to the mediolateral dorsal column midline at the T10 spinal level.

2.2. Computational FEM model solution method

To generate a FEM and correct for some tissue-specific anatomical anomalies (for e.g. overlapping, extrusion, smoothing) using morphological image processing filters, we imported the assembled SolidWorks (Dassault Systemes Corp., MA, USA) CAD model files along with the SCS leads into Simpleware (Synopsis Inc. CA, USA). We generated an adaptive tetrahedral mesh using built-in voxel-based meshing algorithms in Simpleware. We refined the mesh density until additional model refinement produced less than 1% difference the voltage and current density at the spinal cord. The resulting model consisted of approximately 150 million tetrahedral elements. To generate a FEM solution, we then imported the volumetric mesh into COMSOL Multiphysics 5.1 (COMSOL Inc. MA, USA). For each model domain, we assigned the following electrical conductivities based on prior literature: vertebrae (0.04 S m^{-1}), intervertebral disc (0.60 S m^{-1}), epidural space (0.04 S m^{-1}), epidural space vasculature (0.66 S m^{-1}), dura mater (0.037 S m^{-1}), dural sac (0.037 S m^{-1}), intraforaminal tissue (0.004 S m^{-1}), CSF (1.7 S m^{-1}), white-matter (isotropic: 0.1432 S m^{-1} or anisotropic: 0.083 S m^{-1} (transverse) and 0.6 S m^{-1} (longitudinal)), spinal cord vasculature (0.66 S m^{-1}), lissauer's tract (0.276 S m^{-1} or 0.083 S m^{-1} (transverse) and 0.6 S m^{-1} (longitudinal)), gray matter (0.276 S m^{-1}), dorsal and ventral root and rootlets (0.1432 S m^{-1}), DRG (0.1432 S m^{-1}), sympathetic chain (trunk and ganglion) (0.1432 S m^{-1}), thoracic aorta and its branching (0.66 S m^{-1}), peripheral vasculatures (0.66 S m^{-1}), soft tissues (0.004 S m^{-1}), metal electrodes ($4 \times 10^6 \text{ S m}^{-1}$), and lead insulation ($2 \times 10^{-5} \text{ S m}^{-1}$) [2, 3, 7, 39]. We applied boundary conditions to represent bipolar SCS, with a 1 A load condition applied at electrode contact 3 (E3) while grounding electrode contact 5 (E5). We assigned insulating boundary conditions on all external model boundaries and continuity for the internal boundaries. We also assigned floating boundary conditions to the remaining inactive electrodes in the model that assumed an equipotential surface with zero net current. To determine the voltage distributions throughout the model, we then solved the Laplace equation ($\nabla \cdot (\sigma \nabla V) = 0$, where V is potential and σ is electrical conductivity) under a steady-state assumption. To improve solution accuracy, we set the relative tolerance to 1×10^{-6} . Finally, we exported the three-dimensional (3D) extracellular voltage distributions calculated from the FEM and applied these voltage distributions to the axon models described below.

2.3. Multicompartment cable model of sensory Axons

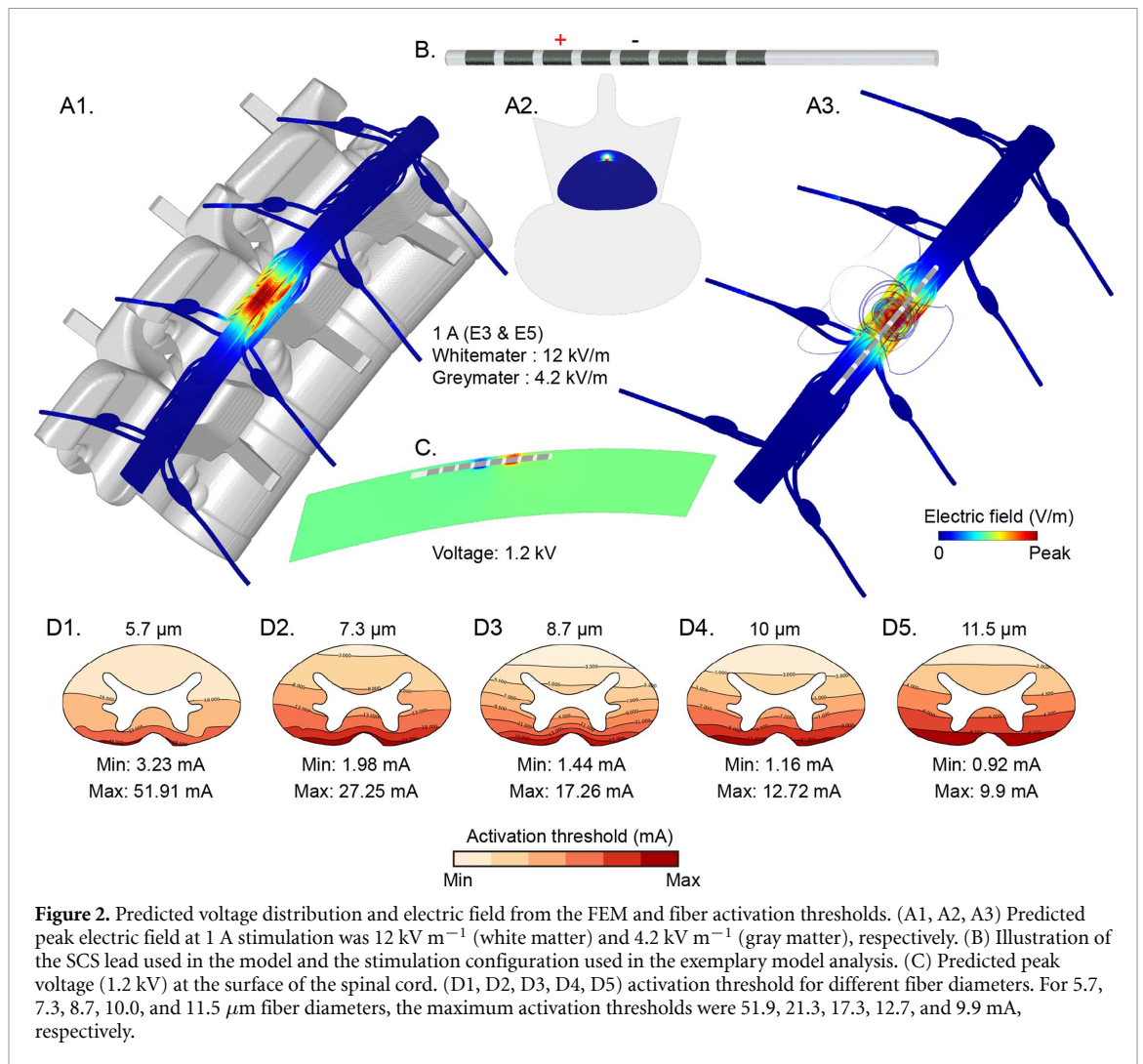
We developed computer models of sensory axons within the dorsal columns of the spinal cord based on a previously-published model of a mammalian sensory axon for specific fiber diameters that were parametrized to reproduce action potential shape, conduction velocity, and strength-duration relationship for sensory axons (figure 1e) [38, 40–42]. Each sensory A β axon model was a double-cable model consisting of nodes of Ranvier separated by three distinct myelin segments: the myelin attachment segment (MYSA), paranodal main segment (FLUT), and the internode regions (STIN).

We distributed the sensory axon models throughout the white matter of the spinal cord using Lloyd's Algorithm [43]. The specific fiber sizes considered in our model matched the diameters explicitly parameterized in a previous study [38]. We calculated the density of fibers in the model using histological measurements of fibers in the most superficial 300 μm of the dorsal columns [44]. To reduce computational demand, we reduced the total number of fibers solved for this project to 1% of anatomic density.

To determine the activation thresholds for each individual fiber, we applied the extracellular voltages calculated in the FEM to our axon models using the software package, NEURON [45], within Python programming environment. We modeled the time-dependent output generated by an implantable pulse generator during current-controlled stimulation. To calculate the appropriate spatiotemporal voltage distributions, we then scaled the time-dependent voltage output by the spatial FEM voltage solution [46, 47]. Using custom made scripts, we applied these extracellular voltages onto the model axons with the extracellular mechanism in NEURON and used a bisection algorithm (error < 1%) to calculate the activation threshold for each axon. In our simulations, we applied a stimulus train consisting of pulses applied at a rate of 50 Hz, pulse width of 300 μs , and a passive discharge phase of 6 ms in duration. We included a total of three pulses in our simulations. To determine the pulse amplitude required to produce tonic firing for each axon, we defined the activation threshold as the lowest pulse amplitude required to generate action potentials for both of the final two pulses of our three-pulse stimulus train. For our sensory axon model, axons that generate action potentials during the final two stimulus pulses will typically continue to generate action potentials at a one-to-one ratio with each stimulus pulse for pulse trains of longer durations.

2.4. General modeling workflow of RADO-SCS

Users can download all STL files of the detailed spinal tissues and prepositioned SCS lead, along with



detailed documentation and current model version, using the weblink provided above. Depending upon the user needs, users can either use all model files (i.e. segmented tissues) or exclude a selection from their model. Users can either customize the model by adding their own electrode/lead or reposition the included lead by using commercial or freely-available CAD software, such as Solidworks (Dassault Systemes Corp., MA, USA), Autodesk (Autodesk, Inc. CA, USA), FreeCAD (<https://www.freecadweb.org>), etc The final model file can then be meshed using commercial software, such as Simpleware (Synopsys Inc. CA, USA), or other open-source packages, such as Gmsh (<http://gmsh.info/>), to generate a volumetric FEM mesh. The mesh can then be imported and solved using a commercial FEM solver, such as COMSOL Multiphysics (COMSOL Inc. MA, USA), or open-source packages, such as SimScale (<https://www.simscale.com/>). The users can then compute the extracellular voltage predicted by the FEM model and couple it with multi-compartment axon models (see [48] for details on how cable models of mammalian nerve fibers are developed) using NEURON (open-source), Python (open-source), or

MATLAB (MathWorks, MA, USA) programming environments to estimate different fiber type activation thresholds.

3. Results

The RADO-SCS model included a total of 245 STL files (including tissues and leads). We further merged alike STL into a single mask using image processing that resulted in 19 tissue masks (millimeter and sub-millimeter dimensions) and four lead masks (two lead types with two masks for each contacts and insulating gap). The resulting volumetric mesh generated after multiple mesh refinements included > 150 million tetrahedral elements requiring 13 h of meshing time on the dedicated supercomputer cluster configured for finite element analysis. Numerically solving the RADO-SCS FEM required an additional 48 h of computing time on the dedicated supercomputer cluster. We then applied the extracellular voltages calculated from the FEM to a population of 2039 model axons located within the DCs of the spinal cord. Developing the axonal models and interpolating the extracellular

voltages took an additional four hours of computing time. The average computing time required to calculate the activation threshold for an individual axon model was typically under one hour, giving a total run time for all fibers of approximately 1672 computational-hours, corresponding to 22 h of real time in cluster computing.

We used an example situation of bipolar stimulation for an exemplary SCS lead positioned epidurally at the targeted lower vertebral spinal levels of the RADO-SCS model and we calculated the voltage and electric field distributions in different tissue compartments. Peak electric fields predicted in the white matter and gray matter were 12 kV m^{-1} and 4.2 kV m^{-1} for 1 A stimulation current, respectively. Peak voltage at the surface of the spinal cord was 1.2 kV (figure 2). The predicted electric field intensities were not uniform in the spinal tissues.

The activation thresholds throughout the white matter are shown in figure 2. As expected, the largest diameter fibers ($11.5 \mu\text{m}$) had the lowest activation thresholds, and the most dorsal fibers were activated at thresholds below 1 mA. As the diameter of the fibers decreased, the activation thresholds increased. The smallest diameter fibers ($5.7 \mu\text{m}$) in the model had a minimum activation threshold of 3.23 mA.

4. Discussion

4.1. Application of state-of-the-art RADO-SCS model

SCS volume conductor models are used for systematic optimization of the design and clinical implementation of SCS technologies, with ongoing efforts to enhance model precision and accuracy. Here, our goal was to develop an open-source high-resolution and anatomically-detailed SCS model and disseminate it to the scientific community. Currently, there is limited access to open-source platforms for SCS modeling, and available models have simple geometries and do not incorporate important tissue compartments. Thus, there is a need to develop and disseminate a high-resolution open-source SCS model. Using our modelling proficiencies, high-end computer resources, and an extensive literature search on anatomical details of spinal cord and peripheral tissues, we developed the first high-resolution open-source SCS model. This model is not only sophisticated in terms of details and architecture, but it also has good precision to predict meaningful current flow. All structural files are freely available to download under the Creative Commons Attribution-Noncommercial International License. In addition, any direct questions regarding the downloadable files or modeling workflow can be directed to the online forum available in the model weblink. Questions will be addressed promptly by the corresponding authors via email. Any new updates will be periodically added

to the source webpage and the model will be periodically checked for any issues.

On one hand, if a user elects to exclude significant details in the RADO-SCS model (e.g. select to use only bone, fat, CSF, and spinal cord masks), the outcome is still a transparent and reproducible structural anatomical pipeline. Whereas on the other hand, the RADO-SCS with its complete complement of tissues provides the opportunity for SCS stimulations with state-of-the-art precision, albeit requiring significant computational resources. The exemplary simulations that we conducted in this study are intended only to illustrate a successful workflow. It is an open question which model details (e.g. vasculature) will significantly impact simulation results, and the answer to this question will moreover depend on the application considered (e.g. electrode placement) and the hypothesized mechanisms of action. Nevertheless, such questions cannot be answered without comparing a precise SCS model with simplified counterparts. In this sense, the RADO-SCS model not only supports models with state-of-the-art precision, but analysis of which model details are ultimately important and which simplifications could be allowed.

While all modeling pipelines reference data from anatomical scans, 'image (MRI) derived models' segment tissue overlaid on medical imaging scans from an individual [2, 46]. MRI-derived models have been increasingly adopted in situations where clinically available scans support individualized models [15, 22, 49]. When models involve incorporation of anatomical details that are not captured within the images (e.g. submillimeter tissue features from imaging scans with only millimeter resolution), then such structures must be rendered by referencing a range of data across techniques and subjects, including cadaver studies. When a majority of modeled tissues are thus rendered, the value of a strictly MRI-derived model (based on an individual scans) becomes unclear. An advantage of fully CAD-derived models is that each tissue is generated based on prescribed geometric features and thus supports reproducibility, systematic alteration, and ongoing refinement.

4.2. Anatomical details of prior SCS models and a need for state-of-the-art open-source SCS model

Finite element analysis has been widely implemented in 2D and 3D spinal cord current flow models. Although a multitude of computational SCS models of rodent and non-human primates has been developed and implemented for motor control following spinal cord injury [50–52], here we specifically focused on human SCS modelling studies (minimally invasive or non-invasive) for pain management. We categorized prior SCS models based on tissue compartments (considered vs. not considered/absent) and anatomical precision (limited, basic precision, moderate precision, and enhanced precision) (see

table 1 for details about these comparison terminologies).

In the early 1980's, Coburn developed the first 2D FEM model representing non-homogeneous human spinal cord tissues for invasive SCS. The model comprised of major spinal tissue domains, such as thoracic vertebrae, epidural fat, CSF, spinal roots, white matter, and gray matter with limited precision [19]. In 1983, Sin and Coburn developed a simplified version of the original Coburn 2D SCS model, excluding spinal roots (limited precision) [53]. Coburn and colleagues in 1985, and Struijk and colleagues in 1991 and 1992 developed 3D FEM models of SCS including major tissues of the spinal canal with basic precision and coarse meshing. In both models, dura was absent, with only Coburn's model including a basic spinal root [20, 31, 54, 55]. Struijk and colleagues in 1993a and 1993b, Holsheimer and colleagues in 1995 and 1997, and Wesselink and colleagues in 1998 and 1999 developed a 3D SCS model including the mid cervical (C4-C6), mid thoracic (T4-T7), and low thoracic (T10-T11) vertebral spine level with major spinal canal tissue compartments, including dura mater and surrounding tissue layers (thorax), all tissue compartments with basic precision [10, 11, 30, 33, 48, 56]. These models simulated either dorsal root (DR) fibers and/or dorsal column (DC) fibers using multicompartment cable models. Wesselink *et al* included white matter anisotropy and encapsulation layer between the electrode and dura [10, 33].

In 2000, Rattay and colleagues developed a T11-L2 SCS model with basic precision in vertebrae, epidural space, dura, CSF, rootlets trajectory, and thorax, whereas the spinal cord (including gray matter and white matter) had moderate precision in anatomical details. They simulated DR fiber activation using a multicompartment cable model [57]. In 2002, Holsheimer used a simplified 3D SCS model that lacked a dura mater compartment (basic precision) to discuss which nerve fibers along the spinal cord were activated by SCS intensities within the therapeutic range [13]. Manola and colleagues in 2005 and 2007 used a basic precision 3D SCS model that included vertebrae, epidural fat, dura, CSF, gray-matter, white-matter, and general thorax in the FEM. They used cable models to simulate DR and DC fiber activation [58, 59]. A more sophisticated CAD-derived SCS model was developed in 2010 by Ladenbauer and colleagues and Danner and colleagues in 2011 for non-invasive and invasive SCS with a vertebral column of moderate precision [28, 60]. This model represented spinal tissue compartments at basic anatomical precision, with uniform dimensions across spine levels. The model also did not include a dura mater in the FEM. The dorsal and ventral root fiber activation were further analyzed using cable models [28]. In 2011, Howard and colleagues developed a simplified 2D SCS model with no dura mater and

limited precision in the modelled tissue compartments [24]. Lee and colleagues in 2011 and Veizi and colleagues in 2017 developed a 3D FEM SCS model of a low thoracic and a sacral level spinal-cord where most tissue compartments had basic anatomical precision, except the spinal cord (whitematter and gray-matter) which had an enhanced precision. They also simulated DR fiber activation using multicompartment cable models [14, 32]. Hernández-Labrado and colleagues in 2011 developed a simplified C2-T1 SCS model comprised of major spinal canal tissue compartments with basic anatomical precision [23]. Parazzini and colleagues in 2014 and Fiocchi and colleagues in 2016 developed an MRI-derived SCS model for non-invasive SCS with enhanced anatomical precision in vertebrae, CSF, and spinal cord; however, other major spinal canal tissue compartments, such as epidural space, dura mater, and roots were not modelled. Moreover, it was unclear whether epidural fat was included in the FEM model [22, 49]. In 2013, Laird and colleagues developed a limited precision SCS model while simulating DC fibers as multicompartment cable models [61]. Howell and colleagues in 2014 constructed a SCS model (lower thoracic/upper lumbar spine level) with moderate anatomical precision in vertebrae, intravertebral disc, dural sac, CSF, white-matter, and gray-matter, and basic anatomical precision in soft tissue (thorax), with tissue compartment dimensions uniform across spine level [25]. In 2014, Huang and colleagues developed a simplified 3D SCS model comprising major spinal canal tissue compartments with basic anatomical precision for epidural and intradural stimulation [26]. In the same year, Kent and colleagues developed another simplified SCS model comprising vertebrae, epidural fat, dura mater, CSF, white-matter, and gray-matter, all with basic anatomical precision [27]. Lempka *et al* 2015 developed a 3D SCS model (lower thoracic spinal cord) of kilohertz frequency SCS with white matter and gray matter with enhanced precision and other tissue compartments with basic anatomical precision [1]. Arle and colleagues in 2014 and 2016 [18, 62] used an FEM derived from the Wesselink [56] and Holsheimer groups' SCS model [30, 55] (basic anatomical precision). In their 2014 SCS model, vertebrae and spinal roots were missing [62]. Fernandes *et al* 2018 and 2019 utilized a MRI-derived human model based on the Virtual Population Family [63] comprising 13 tissue compartments; namely skin, fat (including subcutaneous adipose tissue), muscle, bone, heart, lungs, viscera, vertebrae, IV disc, dura mater, CSF, brainstem, and spinal cord (gray matter and white matter) [15, 16]. The model had enhanced anatomical precision on peripheral spinal tissues/thorax, vertebrae, IV disc, CSF, dura mater, and spinal cord, but basic precision in the roots. It was unclear whether the epidural space (fat) was included in the model.

Durá *et al* 2019 developed a simplified 3D SCS model at the T10 spine level with basic anatomical precision in vertebrae, epidural fat, dura mater, CSF, while both white-matter and gray-matter had moderate anatomical precision. DR fiber geometry included in the FEM had limited anatomical precision [21]. In 2018, Kent and colleagues developed a 3D dorsal root ganglion (DRG) model with basic anatomical precision of the dorsal root and the DRG, and limited precision in epidural tissues and vertebrae [64]. Wagner and colleagues in 2018 constructed a moderate precision SCS model of L1-S2 spine level including epidural fat, CSF, gray-matter, white matter, spinal roots (dorsal and ventral), and rootlets. However, it was unclear whether vertebrae, discs, dura, and thorax were included in the model [65]. Lempka and colleagues in 2019 constructed a patient-specific FEM SCS model with spinal cord, CSF, epidural fat, and a simplified spine domain. All segmented tissue compartments had moderate anatomical precision. They also modeled DC and DR fibers using multicompartment cable models [46, 66].

In 2019, Anderson and colleagues developed a simple 3D SCS model with basic anatomical precision of major spinal canal tissue compartments (white matter, gray matter, CSF, dura, and extradural tissue layer) [5]. A human L5 DRG model with basic anatomical precision was developed by Graham *et al* in 2019 where they represented general thorax, bone, intraforaminal tissue, dural covering, and DRG using simplified shapes [40]. Bikson's group in 2019 developed a simplified T8-T10 SCS model comprising vertebrae (moderate precision), IV disc (moderate precision), epidural space/fat (basic precision), meninges/dura mater (basic precision), CSF (basic precision), spinal cord (basic precision), spinal roots (basic precision), rootlets (basic precision), thoracic aorta and sub-vasculature (basic precision), and soft tissues/thorax (basic precision) [2, 34]. In the same year, Lempka's group developed an updated 3D SCS model of the lower thoracic spine level consisting gray matter and white matter of the spinal cord (enhanced anatomical precision), dorsal rootlets (moderate precision), CSF (basic precision), dura mater (basic precision), epidural fat (basic precision), vertebrae (moderate precision), and discs (moderate precision) [17]. This model had additional details and precision in some tissue compartments compared to their 2015 SCS model, but some major spinal tissue compartments were not included in the model, the dimensions of the tissue compartments were uniform across spinal levels, and the surrounding tissue/thorax had simplified geometry.

Prior SCS studies clearly demonstrate that computational models represent a valuable tool to study the potential mechanisms of action of SCS and to optimize the design and implementation of SCS technologies. However, it is imperative that these computational models include the appropriate level of

details to accurately predict the neural response to SCS and to correlate model predictions with clinical outcomes. Various simplifications to the model design may affect model-based predictions of the neural response to SCS. Therefore, we believe that there is a need for an anatomically-detailed high-resolution spinal cord model that captures major spinal tissue compartments in order to support enhanced prediction of SCS current flow. Here, the RADO-SCS is a state-of-the-art open-source contribution.

Acknowledgments

Source(s) of financial support: This study was partially funded by grants to MB from NIH (NIH-NINDS 1R01NS101362, NIH-NIMH 1R01MH111896, NIH-NCI U54CA137788/U54CA132378, and NIH-NIMH 1R01MH109289), PSC CUNY, Cycle 50.

Conflict of interest

The City University of New York (CUNY) has IP on neuro-stimulation system and methods with author, NK and MB as inventors. MB advises Boston Scientific, GlaxoSmithKline, and Mectra. MB has equity in Soterix Medical Inc. SFL holds stock options with Presidio Medical, Inc. and serves on the scientific advisory board.

ORCID iDs

Niranjan Khadka  <https://orcid.org/0000-0002-4930-5214>

Hans Zander  <https://orcid.org/0000-0001-9720-9553>

References

- [1] Lempka S F, McIntyre C C, Kilgore K L and Machado A G 2015 Computational analysis of kilohertz frequency spinal cord stimulation for chronic pain management *Anesthesiology* **122** 1362–76
- [2] Zannou A L, Khadka N, Truong D Q, Zhang T, Esteller R, Hershey B and Bikson M 2019 Temperature increases by kilohertz frequency spinal cord stimulation *Brain Stimul.* **12** 62–72
- [3] Khadka N, Truong D Q, Williams P, Martin J H and Bikson M 2019 The Quasi-uniform assumption for spinal cord stimulation translational research *J. Neurosci. Methods* **328** 108446
- [4] Peterchev A V, Wagner T A, Miranda P C, Nitsche M A, Paulus W, Lisanby S H, Pascual-Leone A and Bikson M 2012 Fundamentals of transcranial electric and magnetic stimulation dose: definition, selection, and reporting practices *Brain Stimul.* **5** 435–53
- [5] Anderson D J, Kipke D R, Nagel S J, Lempka S F, Machado A G, Holland M T, Gillies G T, Howard M A and Wilson S 2019 Intradural spinal cord stimulation: performance modeling of a new modality *Front. Neurosci.* **13** 253

- [6] Zhang T C, Janik J J and Grill W M 2014 Mechanisms and models of spinal cord stimulation for the treatment of neuropathic pain *Brain Res.* **1569** 19–31
- [7] Zannou A L, Khadka N, FallahRad M, Truong D Q, Kopell B H and Bikson M 2019 Tissue Temperature Increases by a 10 kHz spinal cord stimulation system: phantom and bioheat model *Neuromodulation* (accepted) (<https://doi.org/10.1111/ner.12980>)
- [8] Capogrosso M, Wenger N, Raspopovic S, Musienko P, Beauparlant J, Luciani L B, Courtine G and Micera S 2013 A computational model for epidural electrical stimulation of spinal sensorimotor circuits *J. Neurosci.* **33** 19326–40
- [9] Jensen M P and Brownstone R M 2019 Mechanisms of spinal cord stimulation for the treatment of pain: still in the dark after 50 years *Eur. J. Pain.* **23** 652–9
- [10] Holsheimer J and Wesselink W A 1997 Optimum electrode geometry for spinal cord stimulation: the narrow bipole and tripole *Med. Biol. Eng. Comput.* **35** 493–7
- [11] Struijk J J, Holsheimer J, Barolat G, He J and Boom H B K 1993 Paresthesia thresholds in spinal cord stimulation: a comparison of theoretical results with clinical data *IEEE Trans. Rehabil. Eng.* **1** 101–8
- [12] Holsheimer J 1998 Computer modelling of spinal cord stimulation and its contribution to therapeutic efficacy *Spinal Cord* **36** 531–40
- [13] Holsheimer J 2002 Which neuronal elements are activated directly by spinal cord stimulation *Neuromodulation: Technol. Neural Interface* **5** 25–31
- [14] Lee D, Hershey B, Bradley K and Yearwood T 2011 Predicted effects of pulse width programming in spinal cord stimulation: a mathematical modeling study *Med. Biol. Eng. Comput.* **49** 765
- [15] Fernandes S R, Salvador R, Wenger C, de Carvalho M and Miranda P C 2018 Transcutaneous spinal direct current stimulation of the lumbar and sacral spinal cord: a modelling study *J. Neural Eng.* **15** 036008
- [16] Fernandes S R, Pereira M, Salvador R, Miranda P C and de Carvalho M 2019 Cervical trans-spinal direct current stimulation: a modelling-experimental approach *J. Neuroeng. Rehabil.* **16** 123
- [17] Anaya C J, Zander H J and Graham R D Sankarasubramanian V and Lempka S F 2020 Evoked potentials recorded from the spinal cord during neurostimulation for pain: a computational modeling study *Neuromodulation: Technol. Neural Interface* **23** 64–73
- [18] Arle J E, Mei L, Carlson K W and Shils J L 2016 High-frequency stimulation of dorsal column axons: potential underlying mechanism of paresthesia-free neuropathic pain relief *Neuromodulation* **19** 385–97
- [19] Coburn B 1980 Electrical stimulation of the spinal cord: two-dimensional finite element analysis with particular reference to epidural electrodes *Med. Biol. Eng. Comput.* **18** 573–84
- [20] Coburn B and Sin W K 1985 A theoretical study of epidural electrical stimulation of the spinal cord—Part I: finite element analysis of stimulus fields *IEEE Trans. Biomed. Eng.* **32** 971–7
- [21] Durá J L, Solanes C, De Andrés J and Saiz J 2019 Computational study of the effect of electrode polarity on neural activation related to paresthesia coverage in spinal cord stimulation therapy *Neuromodulation* **22** 269–79
- [22] Fiocchi S, Ravazzani P, Priori A and Parazzini M 2016 Cerebellar and spinal direct current stimulation in children: computational modeling of the induced electric field *Front. Hum. Neurosci.* **10**
- [23] Hernández-Labrado G R, Polo J L, López-Dolado E and Collazos-Castro J E 2011 Spinal cord direct current stimulation: finite element analysis of the electric field and current density *Med. Biol. Eng. Comput.* **49** 417–29
- [24] Howard M A, Utz M, Brennan T J, Dalm B D, Viljoen S, Jeffery N D and Gillies G T 2011 Intrathecal approach to selective stimulation in the spinal cord for treatment of intractable pain: design principles and wireless protocol *J. Appl. Phys.* **110** 044702
- [25] Howell B, Lad S P and Grill W M 2014 Evaluation of intrathecal stimulation efficiency and selectivity in a computational model of spinal cord stimulation *PLoS ONE* **9** e114938
- [26] Huang Q, Oya H, Flouty O E, Reddy C G, Howard M A, Gillies G T and Utz M 2014 Comparison of spinal cord stimulation profiles from intra- and extradural electrode arrangements by finite element modelling *Med. Biol. Eng. Comput.* **52** 531–8
- [27] Kent A R, Min X, Rosenberg S P and Fayram T A 2014 Computational modeling analysis of a spinal cord stimulation paddle lead reveals broad, gapless dermatomal coverage *36th Annual Int. Conf. of the IEEE Eng. Med. Biol. Soc.* pp 6254–7
- [28] Ladenbauer J, Minassian K, Hofstoetter U S, Dimitrijevic M R and Rattay F 2010 Stimulation of the human lumbar spinal cord with implanted and surface electrodes: a computer simulation study *IEEE Trans. Neural Syst. Rehabil. Eng.* **18** 637–45
- [29] Miranda P C, Salvador R, Wenger C and Fernandes S R 2016 Computational models of non-invasive brain and spinal cord stimulation *38th Annual Int. Conf. of the IEEE Eng. Med. Biol. Soc. (EMBC)* pp 6457–60
- [30] Struijk J J, Holsheimer J and Boom H B 1993 Excitation of dorsal root fibers in spinal cord stimulation: a theoretical study *IEEE Trans. Biomed. Eng.* **40** 632–9
- [31] Struijk J J, Holsheimer J, van Veen B K and Boom H B 1991 Epidural spinal cord stimulation: calculation of field potentials with special reference to dorsal column nerve fibers *IEEE Trans. Biomed. Eng.* **38** 104–10
- [32] Veizi E et al 2017 Spinal cord stimulation (SCS) with anatomically guided (3D) neural targeting shows superior chronic axial low back pain relief compared to traditional SCS-LUMINA study *Pain. Med.* **18** 1534–48
- [33] Wesselink W A, Holsheimer J and Boom H B K 1998 Analysis of current density and related parameters in spinal cord stimulation *IEEE Trans. Rehabil. Eng.* **6** 200–7
- [34] Khadka N, Zannou A, Truong D, Zhang T, Esteller R, Hersey B and Bikson M 2019 Generation 2 kilohertz spinal cord stimulation (kHz-SCS) bioheat multi-physics model *Brain Stimul.: Basic Trans. Clin. Res. Neuromodulation* **12** 566
- [35] Kameyama T, Hashizume Y and Sobue G 1996 Morphologic features of the normal human cadaveric spinal cord *Spine* **21** 1285–90
- [36] Geddes L A and Baker L E 1967 The specific resistance of biological material—a compendium of data for the biomedical engineer and physiologist *Med. Biol. Eng.* **5** 271–93
- [37] Bozkurt M, Canbay S, Neves G F, Aktüre E, Fidan E, Salamat M S and Başkaya M K 2012 Microsurgical anatomy of the dorsal thoracic rootlets and dorsal root entry zones *Acta Neurochir.* **154** 1235–9
- [38] McIntyre C C, Richardson A G and Grill W M 2002 Modeling the excitability of mammalian nerve fibers: influence of afterpotentials on the recovery cycle *J. Neurophysiol.* **87** 995–1006
- [39] Chaturvedi A, Butson C R, Lempka S F, Cooper S E and McIntyre C C 2010 Patient-specific models of deep brain stimulation: influence of field model complexity on neural activation predictions *Brain Stimul.* **3** 65–67
- [40] Graham R D, Bruns T M, Duan B and Lempka S F 2019 Dorsal root ganglion stimulation for chronic pain modulates A β -fiber activity but not C-fiber activity: A computational modeling study *Clin. Neurophysiol.* **130** 941–51
- [41] Howells J, Trevillion L, Bostock H and Burke D 2012 The voltage dependence of I_h in human myelinated axons *J. Physiol.* **590** 1625–40
- [42] Gaines J L, Finn K E, Slopsema J P, Heyboer L A and Polasek K H 2018 A model of motor and sensory axon activation in the median nerve using surface electrical stimulation *J. Comput. Neurosci.* **45** 29–43

- [43] Lloyd S 1982 Least squares quantization in PCM *IEEE Trans. Inf. Theory* **28** 129–37
- [44] Feirabend H K P, Choufoer H, Ploeger S, Holsheimer J and van Gool J D 2002 Morphometry of human superficial dorsal and dorsolateral column fibres: significance to spinal cord stimulation *Brain* **125** 1137–49
- [45] Hines M L and Carnevale N T 1997 The NEURON simulation environment *Neural Comput.* **9** 1179–209
- [46] Lempka S F, Zander H J, Anaya C J, Wyant A, Ozinga J G and Machado A G 2019 Patient-specific analysis of neural activation during spinal cord stimulation for pain *Neuromodulation* (accepted) (<https://doi.org/10.1111/ner.13037>)
- [47] Lempka S F, Howell B, Gunalan K, Machado A G and McIntyre C C 2018 Characterization of the stimulus waveforms generated by implantable pulse generators for deep brain stimulation *Clin. Neurophysiol.* **129** 731–42
- [48] Holsheimer J, Barolat G, Struijk J J and He J 1995 Significance of the spinal cord position in spinal cord stimulation *Advances in Stereotactic and Functional Neurosurgery 11* (Vienna: Springer) pp 119–24
- [49] Parazzini M, Fiocchi S, Liorni I, Rossi E, Cogiamanian F, Vergari M, Priori A and Ravazzani P 2014 Modeling the current density generated by transcutaneous spinal direct current stimulation (tsDCS) *Clin. Neurophysiol.* **125** 2260–70
- [50] Capogrosso M, Wenger N, Raspopovic S, Musienko P, Beauparlant J, Bassi Luciani L, Courtine G and Micera S 2013 A computational model for epidural electrical stimulation of spinal sensorimotor circuits *J. Neurosci.* **33** 19326–40
- [51] Capogrosso M et al 2018 Configuration of electrical spinal cord stimulation through real-time processing of gait kinematics *Nat. Protoc.* **13** 2031–61
- [52] Greiner N and Capogrosso M 2019 Anatomically realistic computational model to assess the specificity of epidural electrical stimulation of the cervical spinal cord *Converging Clinical and Engineering Research on Neurorehabilitation III* ed L Masia, S Micera, M Akay and (Berlin: Springer) pp 44–8
- [53] Sin W K and Coburn B 1983 Electrical stimulation of the spinal cord: a further analysis relating to anatomical factors and tissue properties *Med. Biol. Eng. Comput.* **21** 264–9
- [54] Coburn B 1985 A theoretical study of epidural electrical stimulation of the spinal cord—part II: effects on long myelinated fibers *IEEE Trans. Biomed. Eng.* **32** 978–86
- [55] Struijk J J, Holsheimer J, van der Heide G G and Boom H B 1992 Recruitment of dorsal column fibers in spinal cord stimulation: influence of collateral branching *IEEE Trans. Biomed. Eng.* **39** 903–12
- [56] Wesselink W A, Holsheimer J and Boom H B 1999 A model of the electrical behaviour of myelinated sensory nerve fibres based on human data *Med. Biol. Eng. Comput.* **37** 228–35
- [57] Rattay F, Minassian K and Dimitrijevic M 2000 Epidural electrical stimulation of posterior structures of the human lumbosacral cord: 2. quantitative analysis by computer modeling *Spinal Cord* **38** 473–89
- [58] Manola L, Holsheimer J, Veltink P H, Bradley K and Peterson D 2007 Theoretical investigation into longitudinal cathodal field steering in spinal cord stimulation *Neuromodulation: Technol. Neural Interface* **10** 120–32
- [59] Manola L and Holsheimer J 2004 Technical performance of percutaneous and laminectomy leads analyzed by modeling *Neuromodulation: Technol. Neural Interface* **7** 231–41
- [60] Danner S M, Hofstoetter U S, Ladenbauer J, Rattay F and Minassian K 2011 Can the human lumbar posterior columns be stimulated by transcutaneous spinal cord stimulation? A modeling study *Artif. Organs* **35** 257–62
- [61] Laird J H and Parker J L 2013 A model of evoked potentials in spinal cord stimulation *35th Annual Int. Conf. of the IEEE Eng. Med. Biol. Soc. (EMBC)* pp 6555–8
- [62] Arle J E, Carlson K W, Mei L and Shils J L 2014 Modeling effects of scar on patterns of dorsal column stimulation *Neuromodulation: Technol. Neural Interface* **17** 320–33
- [63] Christ A et al 2009 The virtual family—development of surface-based anatomical models of two adults and two children for dosimetric simulations *Phys. Med. Biol.* **55** N23–N38
- [64] Kent A R, Min X, Hogan Q H and Kramer J M 2018 Mechanisms of dorsal root ganglion stimulation in pain suppression: A computational modeling analysis *Neuromodulation: Technol. Neural Interface* **21** 234–46
- [65] Wagner F B et al 2018 Targeted neurotechnology restores walking in humans with spinal cord injury *Nature* **563** 65–71
- [66] Lempka S F, Zander H, Anaya C J, Wyant A, Ozinga J G and Machado A G 2019 Model-based analysis of spinal cord stimulation for chronic pain *Converging Clinical and Engineering Research on Neurorehabilitation III* ed L Masia, S Micera, M Akay and J L Pons (Berlin: Springer) pp 39–43